Assessment of Predictive Capability of Hybrid URANS/LES Methods in Residence Time Calculation

A. Mehdizadeh[1], S. Doost[2], A. Sadiki[2], J. Janicka[2] and N. Karimi[1,3]

[1]School of Computing and Engineering Civil and Mechanical Engineering Department, University of Missouri-Kansas City, MO, USA

[2]Institute of Energy and Power Plant Technology Department of Mechanical Engineering Technische Universität Darmstadt, 64289 Darmstadt, Germany

[3]School of Engineering, University of Glasgow, Glasgow G12 8QQ, United Kingdom

February 15, 2018

Abstract

The present study aims to assess capability of mostly used hybrid URANS/LES methods in dealing with a complex swirled configuration/reactor when the residence time characteristics need to be predicted at acceptable level of accuracy and fidelity. The configuration is quite complex and out of reach of the classical RANS turbulence models as it consists of different, partly swirled inlet channels and a large variety of time and length scales. In this work only the flow field is considered and is investigated using three different hybrid URANS/LES simulation methods. The models: the Scale Adaptive Simulation (SAS), the Improved Delayed Detached Eddy Simulation(SA-IDDES) and the $k-\omega-DES$, use different triggering mechanisms and underlying RANS models. The results of the flow field, the residence time characteristics and all related quantities are compared with both the Large Eddy Simulation (LES) and experimental data reported in

Doost et.al[17]. It turns out that none of the considered hybrid methods is able to predict the residence time characteristics as well as LES does mainly due to the inaccurate prediction of the flow field. It was found that there is a need to improve the hybrid approaches by addressing the shortcomings, particularly those regarding triggering mechanism to make hybrid approaches a reliable computational tool for study complex turbulent flows inside full scale configurations where LES can be prohibitively expensive.

Keywords: Complex swirled flow, Residence time characteristics, Hybrid URANS/LES approach

1 Introduction

Swirled flow configurations are often considered as appropriate generic test cases to assess capability of turbulence models as they are mostly encountered in real engineering applications[23, 24]. Among them, combustion systems recently have attracted a good amount of attention to reduce air pollution as they use generally fossil fuel that leads to produce high amount of pollution[15, 16, 25]. Fossil fuels including coal and natural gas remain inevitable as the major source of energy at least for next decade due to the slow advancement in renewable energy technology development and thus, there is an immediate need to optimize/redesign combustion reactors.

Gas residence time, i.e. the mean time fluid element remains inside the reactor/combustor that provides useful clues on mixing pattern inside the system is one of the key parameters necessary for optimization purposes [32, 31, 33]. In this study, for the first time, hybrid URANS/LES methodology has been applied to predict residence time characteristics inside a complex geometry. Hybrid URANS/LES Methods integrated with the appropriate high performance computing (HPC) techniques are believed to be central to the development of the next generation of prediction/optimization capabilities in a variety of engineering applications. In particular, application of these becomes essential in problems where the excessive cost of full-scale field experiments makes the collection of data practically impossible. The residence time dynamics inside a confined system

can be determined by evaluating of behavior of a passive tracer (introduced at inlet as a pulse or step function) at exit plane of the system[31, 30]. It is worth to mention here that experimental determination of residence time dynamics is very challenging for complex configuration, calling for reliable numerical approaches[30] to study full scale configurations, yet, computationally affordable.

Reynolds averaged Navier-Stokes equation (RANS) models are generally used to simulate stationary high Reynolds number turbulent flows with industrial applications. Unsteady extensions of RANS models (URANS) attempt to capture some level of unsteady dynamics. Since URANS methods are not designed to capture integral-scale dynamics, large eddy simulation (LES) is sometimes needed to capture essential energetic unsteady dynamics in complex flows [1, 19]. Since introduction of LES in the early 1970, it has been significantly advanced, and its application is transitioning from pure academic environment to industry. LES can provide detail information on large scale motion in turbulent high Reynolds number flows. However, LES is not still feasible for many engineering applications due to the high computational cost associated with grid and time step requirements to appropriately resolve the energy containing eddies. This is particularly the case when near wall effects need to be predicted accurately [20, 1]. Another challenge is modeling of sub-grid structure (result of filtering operation) such that to capture complex interaction between large and small scale turbulence. LES could provide inaccurate results if effects of small scale turbulent structures are not appropriately modeled. Therefore, development of advanced models for the unresolved scales that adapt to the local flow conditions and the hybridization of LES with the solution of the Reynolds-averaged Navier–Stokes equations is still an active research area[27]. Hybrid URANS-LES modeling approaches could potentially provide reasonable intermediate strategies by treating near-wall dynamics with URANS while transitioning to scale-resolving (LES) mode away from surfaces with affordable computation costs. The main goal of an URANS/LES hybrid approach is to achieve time dependent and three-dimensional space resolved simulation of large-scale structures, which describe the turbulence dynamics with affordable computational costs. Typically, URANS is applied to capture near-wall dynamics (regions with dimensionless wall distance, y^+,$< (60 - 100)$ concerning wall-bounded attached flows). Small scales turbulence often reside near solid walls and play an integral role in determining the entire flow dynamics. Application

of LES to directly resolve these structures is prohibitively expensive. This necessitates the use of URANS to model these scales. LES is applied away from the solid surface (wall) where viscous effects are negligible and turbulent structures (eddies) are close to isotropic. This allows for the implementation of appropriate mesh without significant increase in computational cost.

Over the last decades, several hybrid URANS-LES approaches have been proposed. Nevertheless two emerging directions have been pursued in parallel, namely zonal and seamless approaches. It is rather straight-forward to identify segregated modeling as a form of zonal coupling and some methods following the paradigm of unified (global) modeling as non-zonal or seamless [35]. In zonal approach, URANS equations are solved in near wall region, while LES equations are solved away from the wall. In both zones, the equations are solved in numerically unsteady mode using a single mesh. Defining the interface location along with matching condition at the interface are the main challenges in the zonal methodology. In unified (seamless) approach a modified RANS model (operating in unsteady mode) is used in entire flow domain and the model decides, on its own, where to operate in URANS or switch to scale-resolving mode. Recent reviews on hybrid methods are reported in [5].

The present investigation aims to study the capability/reliability of three different seamless hybrid modeling strategies (i.e. $k-\omega-SST-SAS$, the SA-IDDES and the $k-\omega-DES$) to predict, first, complex flow field dynamics such as interaction between attached boundary layer with swirled flow and second, residence time characteristics inside a complex swirl chamber. The configuration considered here is similar to the case investigated in [17]. Results will be assessed with respect to high fidelity LES results obtained in [17] using WALE LES model[29] and experimental data[30]. The combustor is designed for the combustion of methane with and without adding coal particles in both air and oxy-fuel environment. The test rig is designed to fill the gap between existing open laboratory-scale coal burners and industry-scale coal combustors with focus on mimicking the near-nozzle region of flame stabilization and combustion of volatiles. In the present study only non-reacting case is considered.

The paper is organized as follows: in the next section the hybrid ($k-\omega-SST-SAS$, $k-\omega-DES$ and $SA-IDDES$) formulations will be shortly presented and discussed. In section three the flow geometry and computational set up of the flow configuration

will be described and the flow field results obtained from different approaches will be presented and discussed. Section four is dedicated to residence time description and discuss related results. Section five will conclude the paper with summary, conclusion and outlook.

2 Hybrid Turbulence Models

In this section we will shortly describe three different hybrid (U)RANS/LES approaches that are mostly used in practice to simulate complex geometries relevant for industrial applications. The main differences between the models are the triggering mechanism to transition from URANS to LES mode and the way near-wall dynamics are treated. It is generally expected that the hybrid models can reliably be applied to flow configurations with sufficiently strong instability available in the base flow (flows with strong swirl/separation)[18]. However, there is no guarantee that the models always deliver accurate results since non of these models qualify for a systematic eddy resolving approach and therefore, they should be applied only to flows for which they have been extensively tested[26]. In the following, we will shortly describe each approach focusing mainly on the triggering mechanisms used in each approach to make a transition from URANS to scale-resolving mode.

2.1 The $k-\omega-SST-SAS$ Model

The Scale Adaptive Simulation (SAS) approach uses the Rotta's equation for integral length scale as a starting point in designing the transition from URANS dynamics to "scale resolving mode," in which the energy dominant integral scales are intended to be resolved conceptually similar to LES. This is achieved by introducing an additional term that includes the second derivative of velocity into the transport equation for ω ($k-\omega-SST-SAS$ [1]). It has been shown that the SAS approach is usually successful in dealing with strongly separated flows and deliver results at an acceptable level of accuracy, and probably is one of the safest hybrid approaches for theses flows [18]
Based on the Rotta equation [11] for turbulence integral length scale, Menter and Egorov

[1] proposed the $SST-SAS$ model by introducing an additional term into the ω transport equation in the $k-\omega-SST$ model [12] in the following form:

$$Q_{SAS} = max\left[\zeta_2 S^2\left(\frac{L}{L_{vk}}\right)^2 - C_{SAS}\frac{2k}{\sigma_\Phi}max\left(\frac{1}{k^2}\frac{\partial k}{\partial x_j}\frac{\partial k}{\partial x_j}, \frac{1}{\omega^2}\frac{\partial \omega}{\partial x_j}\frac{\partial \omega}{\partial x_j}\right), 0\right], \quad (1)$$

where $C_{SAS} = 2$, $\zeta_2 = 1.47$, $\sigma_\phi = \frac{2}{3}$ and L_{vk} represents the von-Karman length scale, defined in terms of the second derivative of velocity as follows:

$$L_{vk} = \kappa\left|\frac{\bar{U}'}{\bar{U}''}\right|, \quad (2)$$

where $\kappa = 0.41$, $\bar{U}'' = \sqrt{\frac{\partial^2 \bar{U}_i}{\partial x_j^2}\frac{\partial^2 \bar{U}_i}{\partial x_k^2}}$ and $\bar{U}' = S = \sqrt{2S_{ij}S_{ij}}$, is the magnitude of the strain-rate tensor. k is turbulent kinetic energy and ω is an inverse turbulence time scale. L is intended to represent a local turbulence length scale. In (U)RANS mode L should represent an integral length scale; but L should reduce to a much smaller value for the simulation to resolve the integral scales when scale-resolving mode is successfully triggered. When the simulation triggers to scale resolving mode, L should, in principle, become the grid scale. Furthermore, Q_{SAS} should trigger the simulation to scale-resolving mode only in regions where grid support is provided appropriately to resolve the integral-scale motions. It has been shown that Q_{SAS} tends to transition from URANS mode to LES when the base flow is sufficiently unstable to trigger a cascade to smaller scale on a grid that should support LES at that location. As a result, the transition from URANS to scale-resolving (LES) mode occurs only in strongly/massively separated flows [2, 1]. Full set of equations is provided in Appendix B.

2.2 The Improved Delayed Detached-Eddy Simulations Model (SA-IDDES)

The detached-eddy simulation methodology is a hybridization of RANS and LES methods with the ultimate goal of improved accuracy and robustness in industrial applications, proposed originally by Spalart et al.[8]. DES is based on a modification of the one-equation RANS model ([8]) turbulent model to dynamically determine the local tur-

bulent length scale and to switch between URANS modeling in attached boundary layers and LES in regions of separated flow. However, in practical applications of the original DES model, grid refinement can result in under-prediction of the wall-stresses or modeled stress depletion (MSD) due to a premature switch from URANS to LES based on the computed length scale. Grid-induced separation (GIS) can be a by-product of this phenomena[9]. Delayed detached-eddy simulation (DDES) was formulated to avoid MSD in ambiguously-refined grids through the introduction of a shielding function that incorporates the eddy viscosity in determining when to switch between the RANS and LES regions [10]. A further extension of the DDES concept is the improved delayed detached eddy simulation (IDDES) proposed by Shur et al.[6]. The objective of IDDES is to combine the benefits of wall-modeled LES (WMLES) and DDES for industrial applications with complex geometry and ambiguous grid refinements. Through shielding functions and solution-based parameters, the model switches between WMLES and DDES. Unlike in the original DES formulation, in IDDES the sub-grid length-scale Δ is a piece-wise function incorporating wall distance dependency and local cell size information:

$$\Delta = min\{max\left[C_w d_w, C_w h_{max}, h_{wn}\right], h_{max}\},$$

where C_w is a constant computed from simulations of the turbulent channel flow, d_w is the distance to the wall, h_{max} is the maximum edge-length of a cell, and h_{wn} is the wall-normal grid spacing. The modified subgrid length-scale accounts for the effects of anisotropic grids that are commonly used in industrial simulations with complex geometry. The formulation results in a significant variation of the length-scale in the flow and often leading to helpful flow destabilization. The model length-scale used in the production term of the eddy viscosity transport equation (see [8] for more detail) is defined as:

$$l_{DDES} = l_{RANS} - f_d max\{0, (l_{RANS} - l_{LES})\},$$

where l_{RANS} is the original length-scale of the Spalart-Allmaras (SA) model and the delaying function f_d is solution-based through:

$$f_d = 1 - tanh[(8r_d^3)],$$

where r_d is calculated as in the original SA model [8]. The LES length-scale l_{LES} is a function of the subgrid length-scale through:

$$l_{LES} = C_{DES}\Psi\Delta,$$

where Ψ is a low-Reynolds number correction function to counteract the activation of the original SA RANS model in the LES regime [7]. The wall-modeled large-eddy simulations (WMLES) branch of IDDES should be activated when unsteady turbulent inflow is provided and if the grid can sufficiently resolve the dominant eddies in the boundary layer. The WMLES length-scale is computed as:

$$l_{WMLES} = f_B(1 + f_e)l_{RANS} + (1 - f_B)l_{LES},$$

where two functions f_B and f_e control the interaction between LES and RANS models. The blending function f_B is designed to improve the switching behavior between LES and RANS based on the distanced to the wall and the local maximum cell edge length:

$$f_B = min\{2exp(-9\alpha^2), 1.0\},$$

where $\alpha = 0.25 - d_w/h_{max}$. The f_e function acts to prevent the log-layer mismatch that can manifest in DES and DDES simulations:

$$f_e = max\{(f_{e1-1}), 0\}\Psi f_{e2}.$$

The f_{e1} term is a function of α and thus it is grid dependent only whereas f_{e2} is a function of the solution by incorporating the term $\sum_{ij}(\partial u_i/\partial x_j)^2$. IDDES combines DDES and WMLES length scale as below:

$$l_{IDDES} = \tilde{f}_d(1 + f_e)l_{RANS} + (1 - \tilde{f}_d)l_{LES},$$

where $\tilde{f}_d = max\{(1 - f_d), f_B\}$.

l_{IDDES} appears in the destruction term of the transport equation for modified eddy

viscosity ($\tilde{\nu}$) as follows:

$$\frac{\partial \tilde{\nu}}{\partial t} + U_i \frac{\partial \tilde{\nu}}{\partial x_j} = c_{b1}\tilde{S}\tilde{\nu} + \frac{1}{\sigma}\left[\bigtriangledown.\left(\tilde{\nu} \bigtriangledown (\tilde{\nu})\right) + c_{b2}(\bigtriangledown \tilde{\nu})^2\right] - c_{w1} f_w (\tilde{r}\left(\frac{\tilde{\nu}}{l_{IDDES}}\right)^2. \quad (3)$$

A detailed description of the IDDES formulation can be found in Shur et al.[6].
Note that in SA-IDDES model (used in the present study), the length-scale in RANS region is the distance from the wall ($l_{RANS} = d_w$).

2.3 The $k - \omega - DES$ Model

The main motivation of developing this model is improvement of separation prediction capability (particularly in mildly separated flow) by improving the underlying RANS model. The mathematical formulation of DES methodology is pretty simple and can be built on any RANS turbulence model. The DES modification based on the $k-\omega-SST$ model is applied to the dissipation term in the k-equation as follows:

$$\frac{\partial \rho k}{\partial t} + U_i \frac{\partial \rho k}{\partial x_j} = P_k - \rho \frac{k^{1.5}}{min(L_t, C_{DES}\Delta)} + D_k \quad (4)$$

where $L_t = \frac{\sqrt{k}}{\beta^* \omega}$, $\Delta = max(\Delta_x, \Delta_y, \Delta_z)$, $\beta^* = 0.09$ is the $k-\omega-SST$ model constant and $C_{DES} = 0.61$ is a calibration constant of the DES formulation. Detailed derivation can be found in [21]. It is worth mentioning here that IDDES is a modified version of DES triggering methodology that only differs in attached flows and performs quite similarly in case of flows with strong instabilities[6]. Moreover, DES methodology and its variants (DDES and IDDES) can be built on any RANS turbulence model (including $k-\omega$ and $k-\epsilon$ frameworks) to develop a hybrid model.

3 Residence Time

3.1 Residence Time Distribution (RTD)

Dealing with complex flows inside reactors/combustors, the characteristic time a fluid particle stays inside the specific system(specific zone inside the system) is of great in-

terest as it provides useful information on mixing pattern denoted as τ_0. For ideal flow conditions without recirculation or axial diffusive transport, e.g., plug-flows in pipes, τ_0 can be determined from the ration of the system volume (V_{sys})to the total volumetric flow rate ($\dot{V}_0$),i.e. $\tau_0 = \frac{V_{sys}}{\dot{V}_0}$[28]). Since each individual fluid element in a non-ideal system has different streak line and velocity, there is need for statistically defined residence time distribution $E(t)$. Experimentally, the residence time distribution (RTD) can be determined by stepwise increasing the concentration of a non reactive tracer introduced at the inlet of the system from 0 to C_f. The non-dimensional cumulative distribution function $F(t)$ is then determined from the temporal evolution of the tracer concentration $C(t)$ at the system outlet, normalized by its steady-state (Theoretical mixed) concentration C_0:

$$F(t) = \frac{C(t)}{C_0}. \tag{5}$$

Note that the value of C_0 at the outlet is determined by dividing the volumetric flow rate of the tracer by the total volumetric flow rate.

The cumulative distribution function (CDF) describes the probability for a fluid element that was injected into the system at $t = 0$ to exit the system between 0 to t . The RTD and the CDF are related to each other by:

$$E(t) = \frac{dF(t)}{dt}. \tag{6}$$

The mean residence time of a real system (denoted by τ) can be calculated by the first-order moment of the RTD as follows:

$$\tau = \int_0^\infty E(t) \times t dt. \tag{7}$$

It is a common practice to assess the second moment (variance) of RTD that provides some idea on spread of distribution. IT is defined as below:

$$\sigma^2 = \int_0^\infty (t - \tau).E(t) dt \tag{8}$$

4 Flow configuration and computational setup

In the present study a complex swirled flow (can also be regarded as a generic test case for oxy-flame combustor [17]) is considered to assess capability of different hybrid methods in predicting flow field and residence time characteristics. Figures 1 and 2 show two different views of the investigated configuration, demonstrating all inlets and the outlet along with a $2D$ plane of the combustor. The geometrical design of the burner nozzle, the quarl, and the expansion to the chamber is similar to the self-sustained oxy-coal flame presented in Toporov et al.[14]. The down fired chamber is also derived from Toporov et al.[14], however, it is shorter and only $600mm$ long. The cross section is square for better optical access with rounded edges for easier meshing. The nozzle consists of a primary inlet at the center with a bluff body where fuel and oxidizer are injected. There are secondary inlets for air/oxidizer designed using channels in annular tubes leading to axial and radial (inclined) (45° relative to the axial) inlets into a plenum in order to generate a relatively strong swirl (0.79 at the diffuser inlet only for secondary flow and 0.47 combined for primary and secondary flow). All (secondary) inlets have a rectangular cross section (axial: $7.5 \times 11.5mm^2$, inclined: $5 \times 8.5mm^2$). The nozzle is connected to the main chamber with a diffuser to allow the swirl to form a stable recirculation zone. The chamber cross section is $420 \times 420mm^2$ and its length is reduced to $600mm$ to decrease residence times and thus, the computational costs. The main sections of the walls are made of plane quartz windows to provide full optical access throughout the chamber. Therefore, the cross section is rectangular, however, with rounded corners to simplify the application of structured meshes. Similar to [14], close to the wall a tertiary annular inlet for the oxidizer is placed at larger radii and is directly connected to the main chamber. The outlet is an annular orifice positioned close to the wall that prevents any back-flow and secondary air entrainment into the main chamber due to extended re-circulation zones.

As mentioned previously, we apply three different hybrid approaches to the present swirled configuration. Results will be compared with experimental data and LES results reported in Doost et al.[17]. They performed a comprehensive mesh dependency study and have shown that a grid with slightly more than 1 million carefully designed hexahedral cells is fine enough to capture the essential dynamics of flow at acceptable level of

Inlet	Velocity(m/s)
Primary	13.1825
Secondary (Axial)	5.23
Secondary (Radial)	15.008
Tertiary	1.7174

Table 1: imposed velocity at each inlet

accuracy.

In the present study only the flow field behavior is studied. Combustion is not considered, i.e. air will be injected with different velocities given in table 1 through each inlet similar to the experiment[30]. Turbulence intensity at the inlets is assumed to be low and around 1% according to the experimental conditions. Non-slip and outlet boundary conditions are applied at the walls and outlet, respectively. It should be noted that the outlet boundary condition applied at the exit ring imposes zero gradient condition and best resembles the experimental situation.

The structured computational grid used here consists of slightly more than 1 million carefully designed hexahedral cells (Same grid used in Doost et al.[17] calculations) and is fine enough to capture essential dynamics of the flow (Fig. 1) as confirmed in Doost et al.[17] in their LES calculations. Doost et al.[17] used WALE model[29] model and performed a comprehensive mesh dependency study with the conclusion that the present mesh is fine enough to capture essential dynamics of the flow/residence time characteristics. This makes the current geometry a suitable test case to assess capability of different hybrid models to deal with complex flows at affordable computation cost. The details of the Wale LES model have been briefly discussed in Appendix A. In order to determine the residence time characteristics to validate/assess the numerical results, similar to [17], the following transport equation for dimensionless passive scalar ϕ is solved to assess the tracer behavior.

$$\frac{\partial \phi}{\partial t} + U_i \frac{\partial \phi}{\partial x_j} = \frac{\partial}{\partial x_j} \left(\left(\frac{\nu}{Sc} + \frac{\nu_t}{Sct} \right) \frac{\partial \phi}{\partial x_j} \right), \tag{9}$$

where ν, ν_t, $Sc = 0.7139$ and $Sc_t = 0.7139$ are molecular viscosity, turbulent eddy viscosity, laminar and turbulent Schmidt numbers respectively.

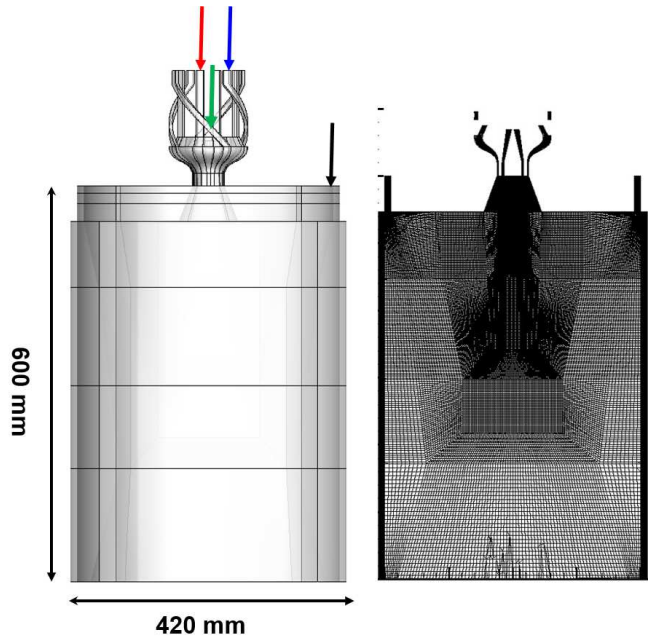

Figure 1: 3D and 2D views of the oxy-fuel configuration displaying inlets and grid in a qualitative fashion

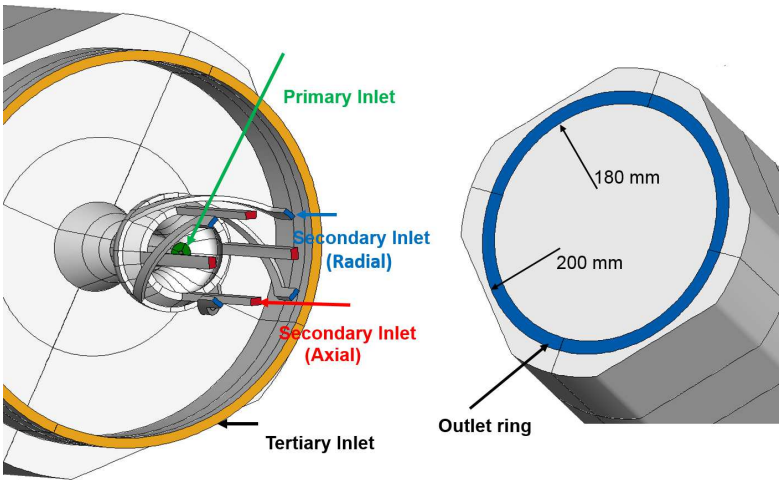

Figure 2: Schematic of inlets and outlet of the oxy-fuel combuster

4.1 Numerical Method

The $3D$ simulations were performed using the open source CFD code, OpenFOAM[13], with second-order central differencing discretisation for velocity and turbulent kinetic energy, k. However, first order upwind scheme was necessary to use to discretize ω to suppress numerical instability. Second order time discretisation method was used for all simulations. Maximum allowed CFL number for entire domain was set to 6 that results mean CFL number well below one in the domain. It is worth mentioning that in LES calculations[17], maximum CFL number needs to remain around one to maintain numerical stability. The unsteady SIMPLE algorithm was applied to advance momentum along with PISO algorithm to solve the pressure Poisson equation.

5 Results and Discussion

5.1 Flow Field

Figures 3 and 4 indicate the plane locations where we compare our numerical results with experimental and LES data and the shear layer (in a qualitative fashion) that forms after the flow separates from the wall and enters the main chamber respectively. It is expected that the models switch into LES mode in separated regions (immediately after the diffuser exit) and start to resolve the turbulent structures. To study the state the models operate in, we compare the eddy viscosities obtained from all three models with the ones of the LES at these three planes (Figure 5). It can be seen that at the first plane ($x = 7mm$) the eddy viscosity obtained from the $SST-SAS$ and the $k-\omega-DES$ models are at least one order of magnitude larger (same order of corresponding URANS eddy viscosity (not shown here)) than the LES eddy viscosity, while the eddy viscosity obtained from the SA-IDDES model undergoes a huge drop and has similar order as LES, meaning that the first two models are operating in URANS mode. This confirms that first two models are not sensitive enough to respond promptly to the internal instability mainly caused by the change in the geometry which might be due to the diffusive nature of the underlying RANS model. Further downstream (at $x = 67mm$ and $x = 167mm$),

both, the $SST-SAS$ and the $k-\omega-DES$ models start transitioning from URANS to scale-resolving mode and a noticeable reduction in the eddy viscosity can be observed. However, the reduction observed in the eddy viscosity obtained from the $SST-SAS$ model does not seem to be enough to drive the model into full scale-resolving mode but to a partially resolving mode around the second plane. Figure 6 demonstrates the spanwise component of instantaneous vorticity obtained from the $SAS-SAS$, LES, SA-IDDES and the $k-\omega-DES$ simulations respectively. It clearly can be seen that consistent with the eddy viscosity behavior, the $SST-SAS$ and $k-\omega-DES$ indicate a very similar response up to about $x=60mm$ and transition to scale-resolving mode is delayed while the SA-IDDES (similar to LES) tries to resolve turbulent structures already from inside the diffuser. Based on the observation mentioned above, it is expected that SA-IDDES delivers results similar to LES on all three planes. Figure 7 demonstrates iso-surface of instantaneous pressure colored by velocity magnitude. It confirms behavior of diffrent models in transition to LES-like mode observed in instantaneous vorticity and the eddy viscosity as discussed above. Furthermore, it may be concluded that having more advanced RANS model for near-wall area (the $SST-SAS$ and the $k-\omega-DES$ models) would cause a delay in the model to response promptly to a change in flow state probably due to the diffusive nature and insensitivity to internal instability of the $k-\omega-SST$ model, while using a very simple near wall model (distance from the wall in the SA-IDDES model) appears to be more sensitive. However, it should be noted that being able to transition to scale-resolving mode is only one part of the triggering mechanism and the second part is that if the model can operate as an appropriate sub-grid scale model after transion to scale resolving mode. We will discuss it by analyzing the statistical quantities in the following.

Figures $8-10$ show the streamwise and the radial mean velocities at three different planes. It can be seen that all three models fail to predict the peak in the streamwise mean velocity at the first plane. In fact, the situation for SA-IDDES is worst and a severe deviation can also be observed around the shear layer. The radial velocity is better predicted and all models deliver results close to the experiment and LES. This outcome is ,however, not expected given that the SA-IDDES model operates in scale-resolving mode at the first plane. It would mean that the second part of the triggering is not happening appropriately. It may lead to the conclusion that the characteristic length and time

scales do not correspond to appropriate sub-grid scales when the model is operating as sub-grid scale model, mainly due to the lack of direct tie to the grid. This is consistent with the discussion provided in [22, 26] regarding uncertainties concerning the seamless hybrid methods when operating in scale-resolving mode. They cannot be considered systematic eddy-resolving methods and therefore, may produce unrealistic spectrum in some situations. Moreover, using a very simple RANS model (distance from the wall) to cover the near-wall dynamics could impact the results severely. Further downstream at the second plane, where almost all three models are operating in full(or partially) scale-resolving mode, results are closer to LES and experiment. At the third plane the situation becomes worse for all three models. As can be observed all three models fail to predict the mean velocities and there is a severe deviation from the reference data. Figure 11 depicts the turbulent kinetic energy. A consistent behavior can also be observed. At the first plane the $SST - SAS$ and the $k - \omega - DES$ models basically deliver typical (U)RANS results, which means that most part of the turbulent kinetic energy is modeled with a severe over-predication of the peak. For the SA-IDDES model, in contrast, almost the turbulent kinetic energy is entirely resolved with notifiable over-prediction exactly in regions where severe deviations (from the reference data) in the mean velocity profiles were observed. Further downstream situation gets better and all models return reasonable results.

5.2 Residence Time Distribution

Results obtained for residence time distribution (RDT) function and its characterization using different hybrid approaches will be discussed and compared with the available LES and experimental data. The main goal here is to determine the interplay between flow field prediction and the RDT prediction accuracy.

Figure 12 compares the cumulative residence time distribution ($F(t)$) obtained from different models at three different locations ($x = [118, 318, 508]mm$). These profiles describe actually the mean concentration growth at the 2D planes perpendicular to the chamber center axis at given locations. It can be observed that non of the hybrid methods is able to deliver results as accurate as LES does regarding overall trend of the function. Furthermore, all three hybrid approaches significantly overestimate the death time, the

time required for tracer after introduction at inlet, to start interacting with the flow field at given location. The situation is worse especially at second and third planes. This may lead to the conclusion that the hybrid methods are not responding to the tracer promptly as LES does which likely lies on inappropriate/incomplete transition to scale-resolving mode associated with all three approaches which prevents effective interaction between the flow field and the tracer.

5.2.1 RTD Characteristics

Regarding RDT characteristics, we evaluate our results obtained from different hybrid approaches with respect to the LES results. Since there is no experimental date available, LES results presented in [17] are considered as the reference data to evaluate/assess the results obtained from hybrid approaches. Note that in figures SA-IDDES will be shown with the IDDES.

Figures $13 - 14$ demonstrate the cumulative and the external residence time of the entire system by obtained by normalizing the tracer concentration at outlet using C_0 as discussed earlier (Eq. (5) and (6)). The top part of each figure shows the cumulative distribution function along with the system death time (time necessary to observe first tracer response). It is clear that the system death line is severely over-predicted by all three hybrid approach relative to the LES prediction. The main reason is thought to be lack of appropriate transition to scale-resolving mode which hampers effective interaction between flow structures and the passive scalar and therefore, prevents the tracer to respond promptly. The middle parts of the figures depict the external residence time distributions ($E(t)$) that are indicator of the mean flow structures inside the reactor/chamber[34]. It can be seen that $E(t)$ obtained from SA-IDDES shows pretty much similar overall behavior as LES, particularly in capturing a peak around $t = 1s$. This is caused by the primary stream the tracer mixing with secondary stream and circumventing the re-circulation areas where the tracer mixes partly inside the re-circulation zone and partly outside of these zones. However, SA-IDDES models predicts two additional peaks around $t = 4.5, 5.5s$ that is related to the inaccurate predictions in the velocity fields presented in the previous section. In contrast, the $SST - SAS$ and the $k - \omega - DES$ models indicate completely inconsistent behaviors by indicating several

peaks suggesting inaccurate prediction of the flow field.
This is again mostly due to the inconsistent/incomplete transition to the LES mode that directly affects the flow field prediction accuracy. The bottom parts of the figures 13, 14 demonstrate the mean residence time (τ). Again, hybrid models fail to predict it accurate enough compared to the LES result.
Figures 15, 16 show the residence time variance obtained from different models. Similar to other quantities, they confirm inaccurate predictions of hybrid methods for the system death time and the system mean residence time and more importantly, physically inconsistent result obtained from the $k - \omega - DES$ model.

5.2.2 Tracer Concentration at Outlet

Finally, the tracer concentration at the outlet as function of time and also, the tracer concentration distribution (relative histogram) for times $t = \tau$ (system mean residence time) and $t = 5s$ are shown in figures 17, 18, 19, 20 using $C_0 = 0.13$ as steady-state value for tracer concentration at outlet. As expected, the distribution patterns of hybrid is different compared to the LES distribution. More importantly, unlike LES, the value of C/C_0 around which the tracer concentration is wildly distributed does not correspond to the absolute concentration at outlet at time close to the system mean residence time (τ).
Based on the results, it is hard to avoid the conclusion that there is a strong interplay between the flow field prediction accuracy and the prediction of the RDT characteristics at acceptable level of accuracy.

6 Summary and Conclusion

Three different hybrid models have been applied to the present complex swirled configuration including various flow dynamics. It was shown that all three approaches have some difficulty dealing with the present configuration. In particular, they fail to respond appropriately to a change of flow state caused by sudden change in the geometry. The

main shortcoming most likely lies in the triggering mechanisms. Models either do not trigger promptly as they should or if triggered do not act as an appropriate sub-grid model, since there is not direct relation to the grid. As shown, it might be the main reason for the observed disagreement with the reference data (LES/Experiment). Moreover, it has been determined that there is a direct link between flow field prediction accuracy and residence time (characteristics) prediction quality. There is a need to modify the triggering mechanism in order to make the all three methods capable/reliable to deal with different flow situations. Maybe using more advanced underlying RANS models (non-linear eddy viscosity models) that are more sensitive to change in flow state along with introduction the grid scale into model when operating in scale-resolving mode are necessary to make appropriate transition from URANS to LES possible and to allow the model to responds promptly and appropriately to a change in flow condition. This is a work-in-progress issue and will be addressed in the future.

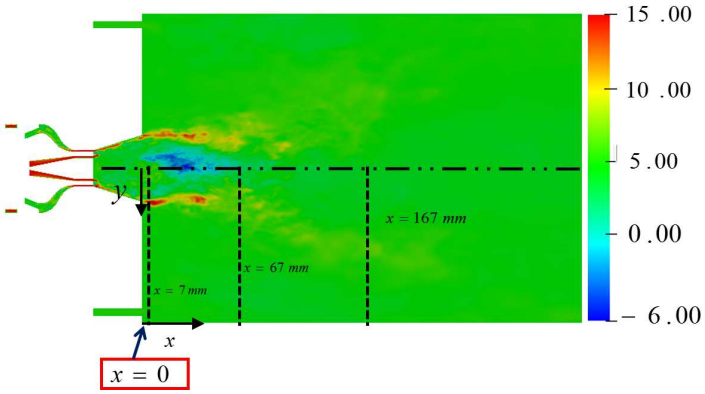

Figure 3: Different measurement planes with instantaneous velocity field obtained from the LES at Time=3s

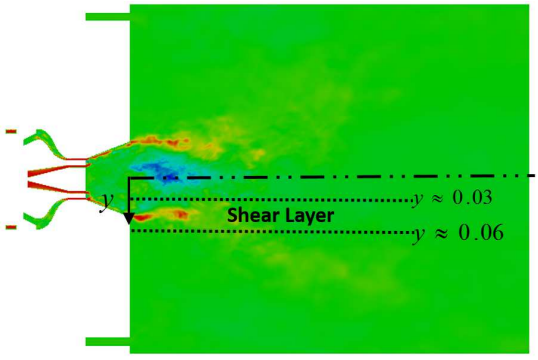

Figure 4: Qualitative schematic of the shear layer inside the combustion chamber shown on velocity field obtained from the LES at Time=3s.

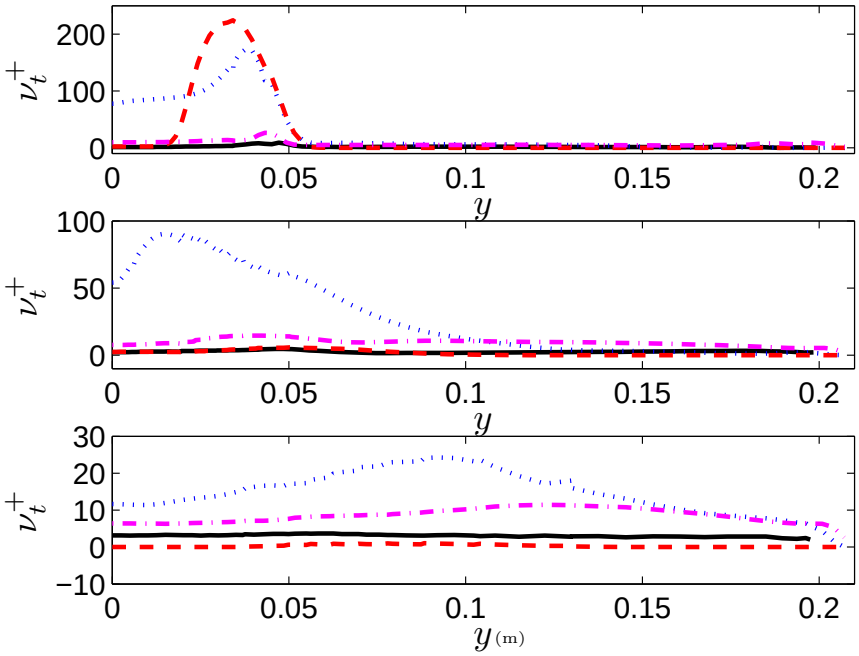

Figure 5: Normalized (using molecular viscosity) mean eddy viscosity at different planes: at different planes: $x = 7mm$ (top), $x = 67mm$ (middle), $x = 167mm$ (bottom), LES:—–, $SST - SAS$: :, SA-IDDES:-·-·, $k - \omega - DES$:- - - -,

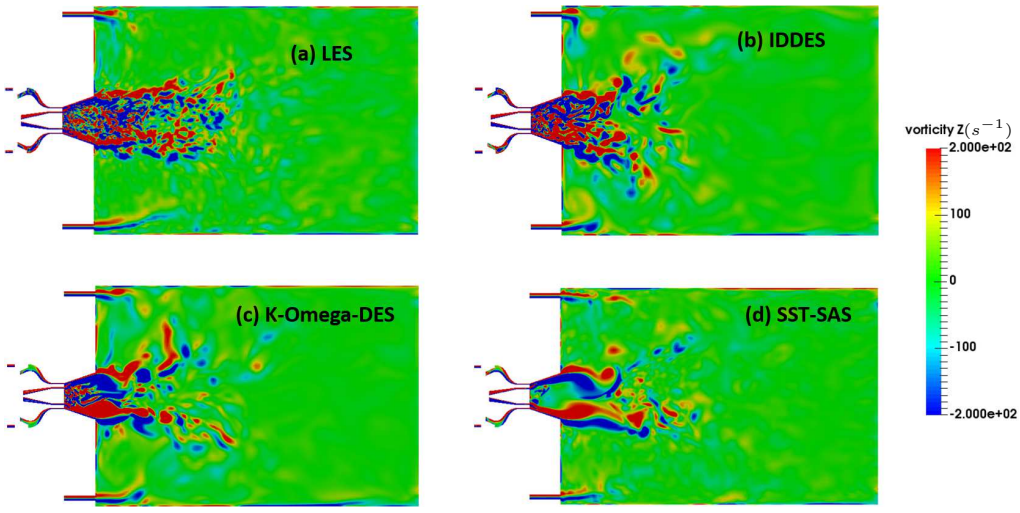

Figure 6: Instantaneous spanwise component of vorticity in a 2D plane obtained at Time=4s.

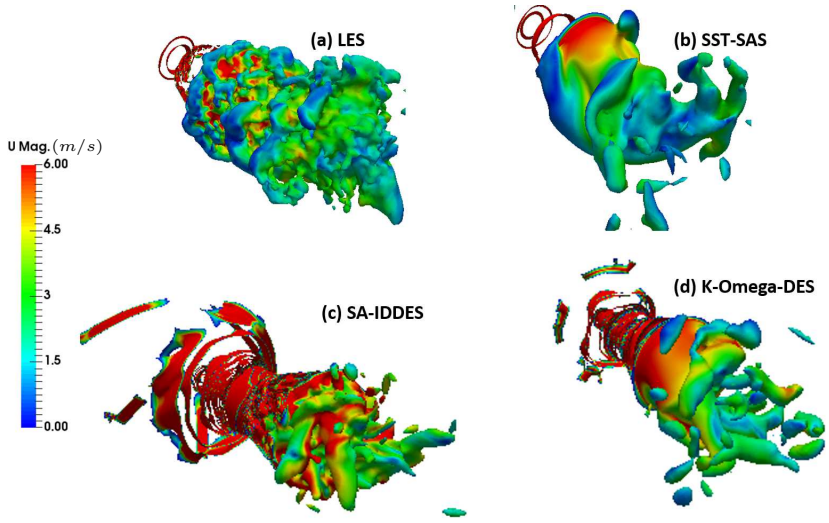

Figure 7: Iso-surface of instantaneous pressure colored by velocity magnitude obtained at Time=4s.

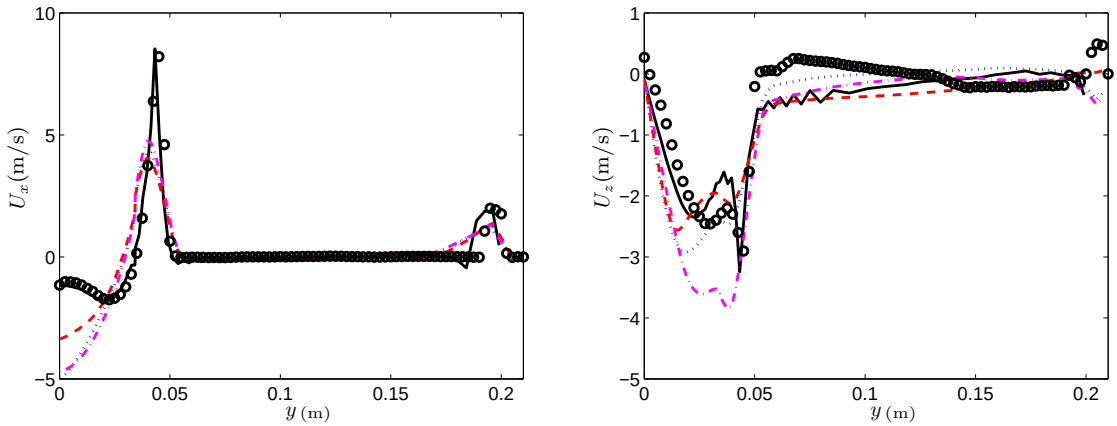

(a) (b)

Figure 8: The stremwise (a) and radial (b) mean velocity profiles (m/s) at different planes: at different planes: $x = 7mm$, $x = 67mm$, $x = 167mm$, LES:——, $SST - SAS$: :, $SA - IDDES$:-·-·-, $k - \omega - DES$:- - - -, Exp.:○..

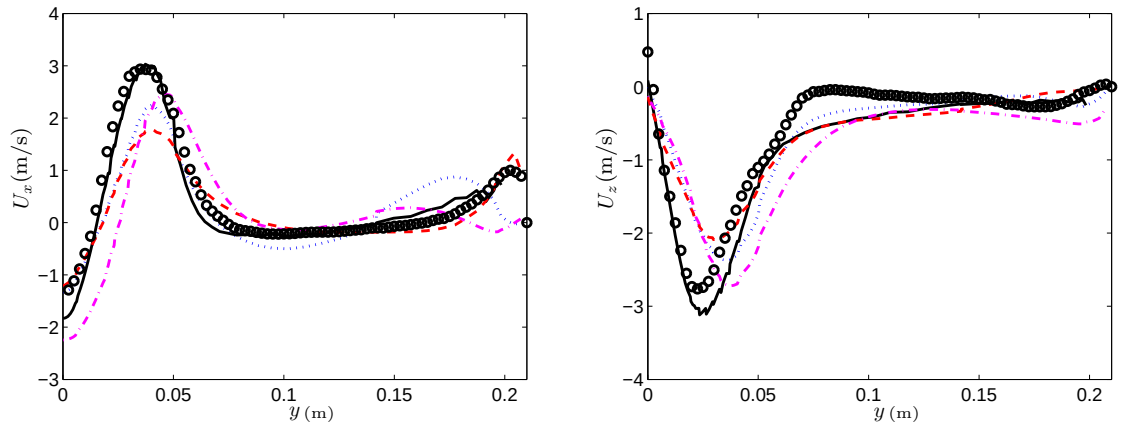

(a) (b)

Figure 9: The stremwise (a) and radial (b) mean velocity profiles (m/s) at different planes: at different planes: $x = 7mm$, $x = 67mm$, $x = 167mm$, LES:——, $SST - SAS$: :, $SA - IDDES$:-.-., $k - \omega - DES$:- - - -, Exp.:○.

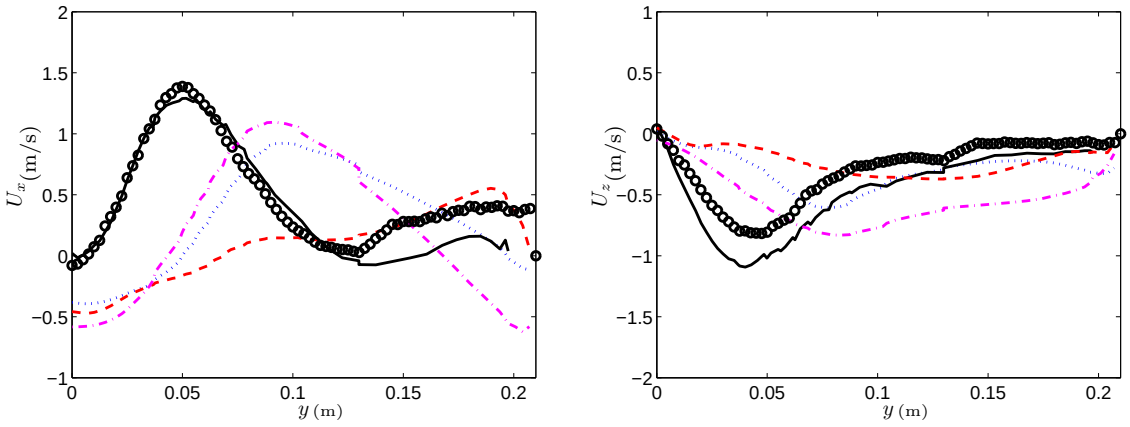

(a) (b)

Figure 10: The stremwise (a) and radial (b) mean velocity profiles (m/s) at different planes: at different planes: $x = 7mm$, $x = 67mm$, $x = 167mm$, LES:——, $SST - SAS$: :, $SA - IDDES$:-.-., $k - \omega - DES$:- - - -, Exp.:○.

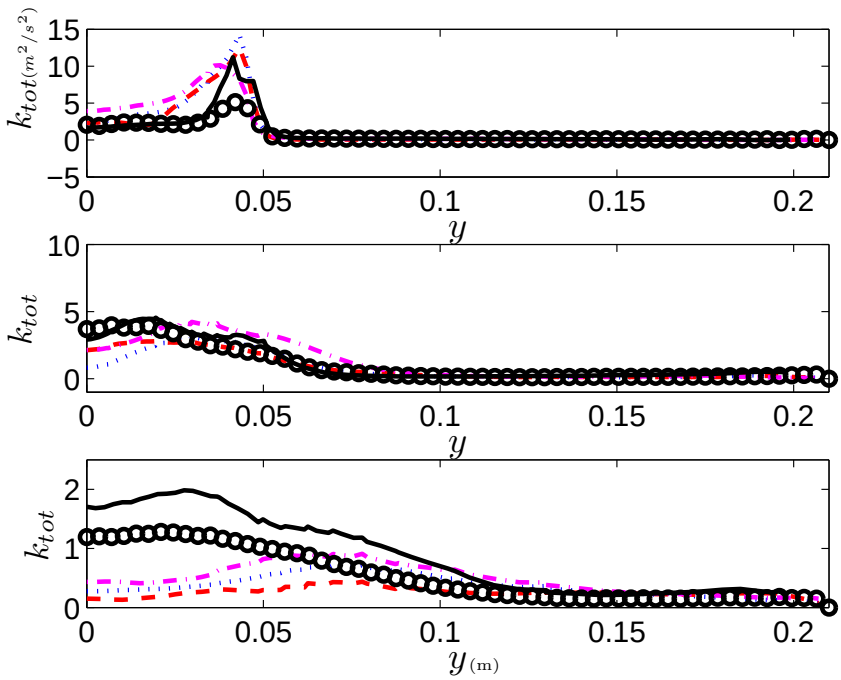

Figure 11: Turbulent kinetic energy (m^2/s^2) at different planes: $x = 7mm$ (top), $x = 67mm$ (middle), $x = 167mm$ (bottom), LES:——, $SST - SAS$: :, $SA - IDDES$:-·-·, $k - \omega - DES$:- - - -, Exp.:○.

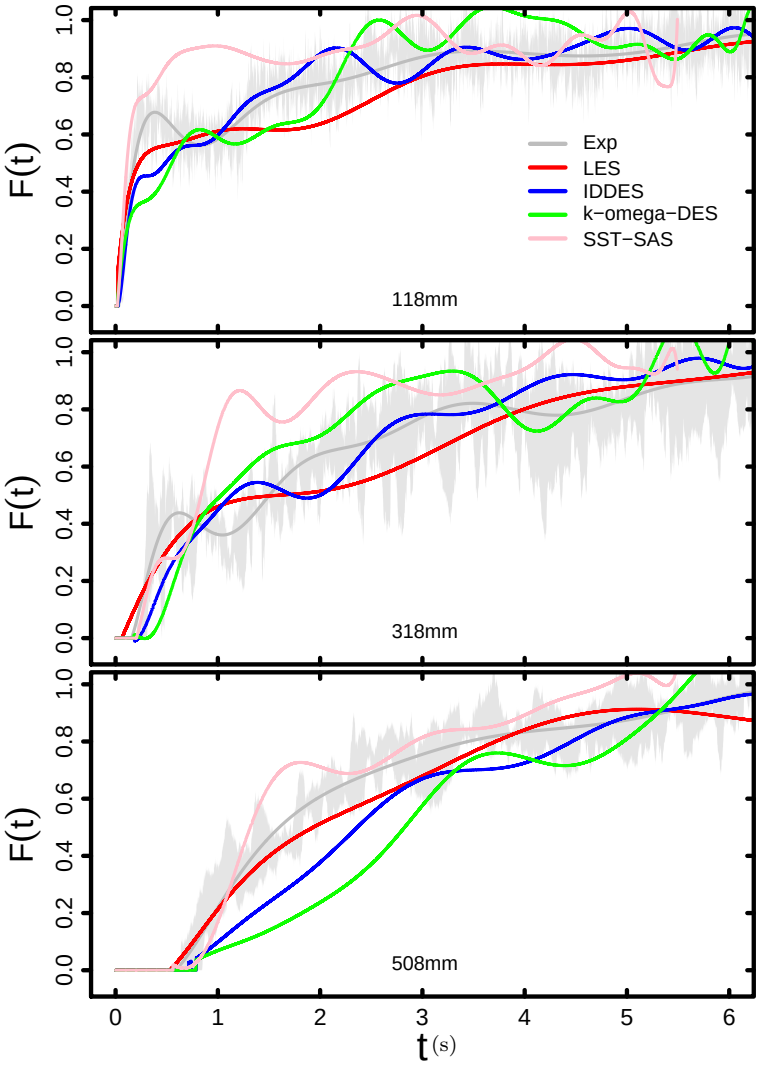

Figure 12: Cumulative residence time distribution $F(t)$ at different planes: LES:——, $SST-SAS$: ——, SA-IDDES:——, $k-\omega-DES$:——, Exp.: ——, Gray area: max/min experimental range.

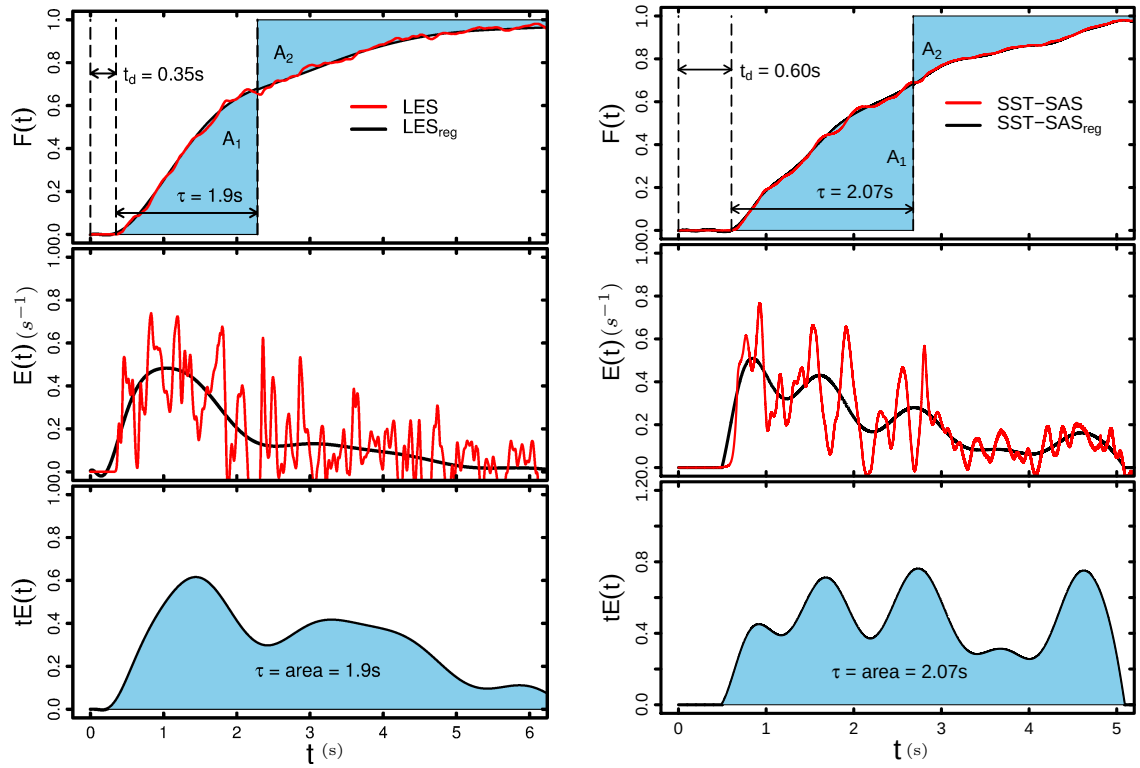

(a) (b)

Figure 13: Cumulative residence time distribution function $F(t)$ (top),external RTD $E(t)$(middle)and external RTD multiplied by time $tE(t)$ (bottom); illustrating the death time t_d and mean residence time τ. (a): WALE model, (b): SST-SAS model, Black line:unsteady data at outlet, red line:regression of data.

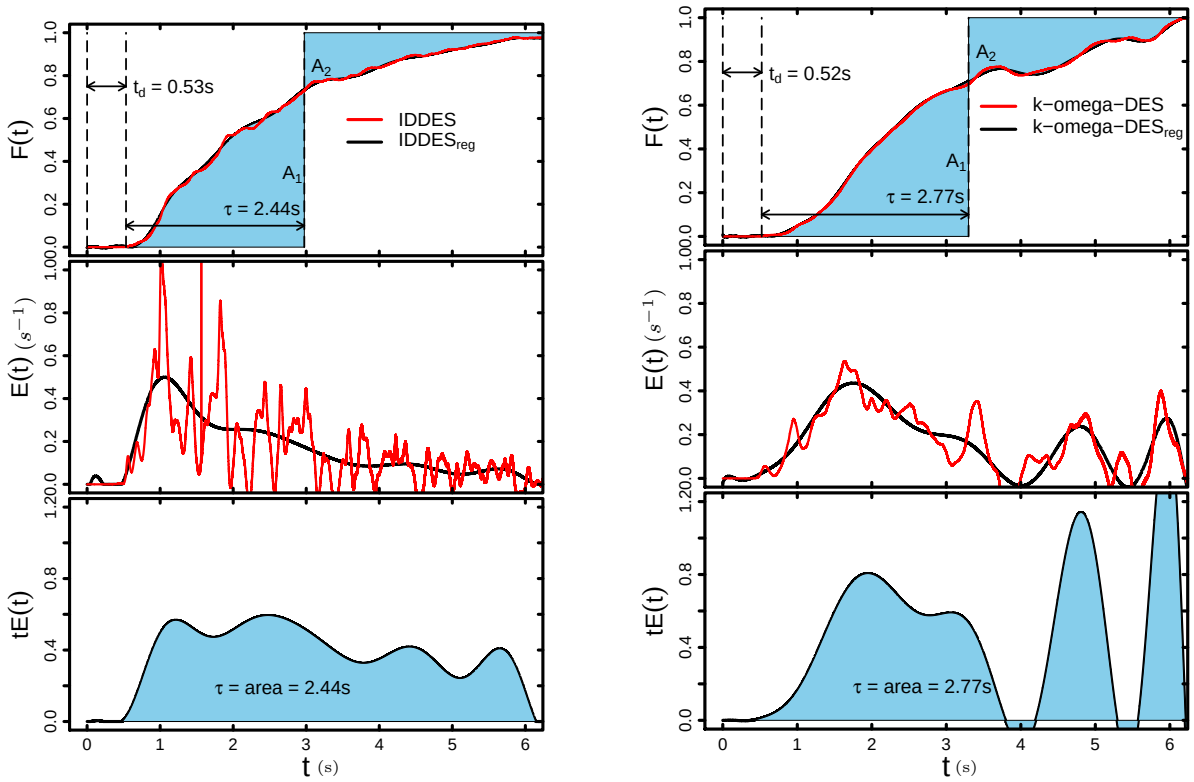

(a) (b)

Figure 14: Cumulative residence time distribution function $F(t)$ (top),external RTD $E(t)$(middle)and external RTD multiplied by time $tE(t)$ (bottom); illustrating the death time t_d and mean residence time τ. (a): SA-IDDES model, (b): k-omega-DES model, Black line:unsteady data at outlet, red line:regression of data.

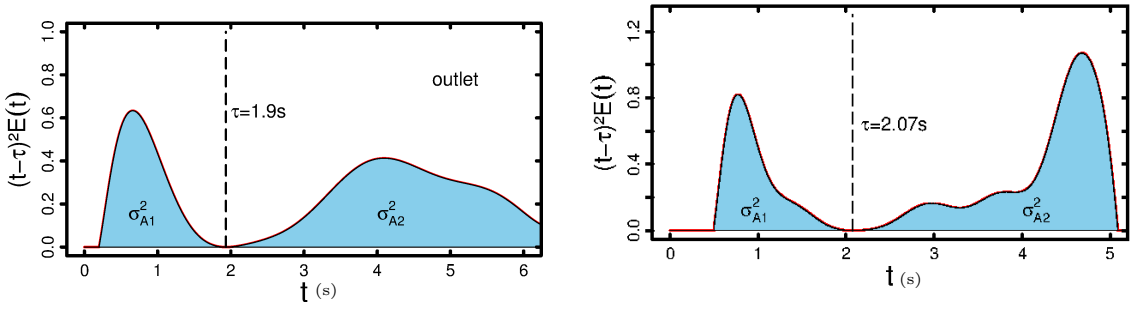

(a) (b)

Figure 15: Distribuation of the residence time variance $(t-\tau)^2E(t)$(s) at outlet, (a): WALE, (b): SST-SAS.

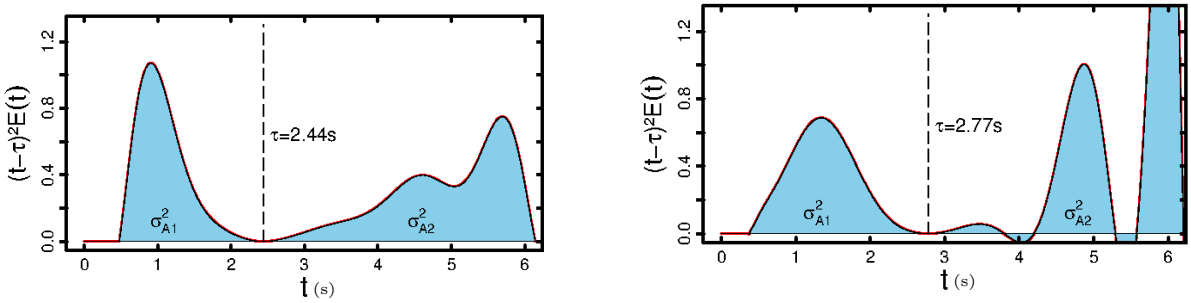

(a) (b)

Figure 16: Distribuation of the residence time variance $(t-\tau)^2 E(t)$(s) at outlet, (a): SA-IDDES, (b): k-omega-DES.

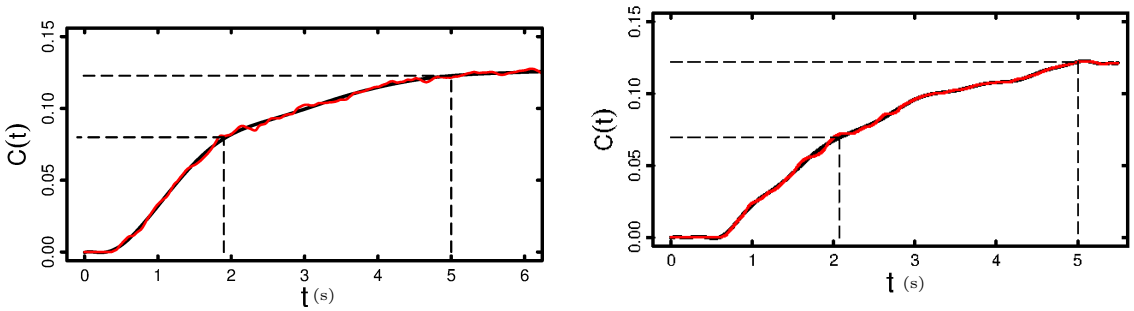

(a) (b)

Figure 17: Exit tracer concentration at outlet C(t) marked at t=[τ, 5]s, (a): WALE , (b): SST-SAS.

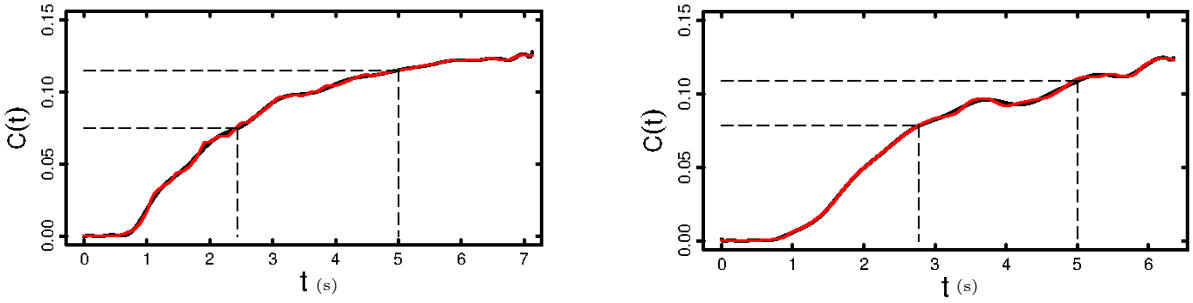

(a) (b)

Figure 18: Exit tracer concentration at outlet C(t) marked at t=[τ, 5]s, (a): SA-IDDES , (b): k-omega-DES.

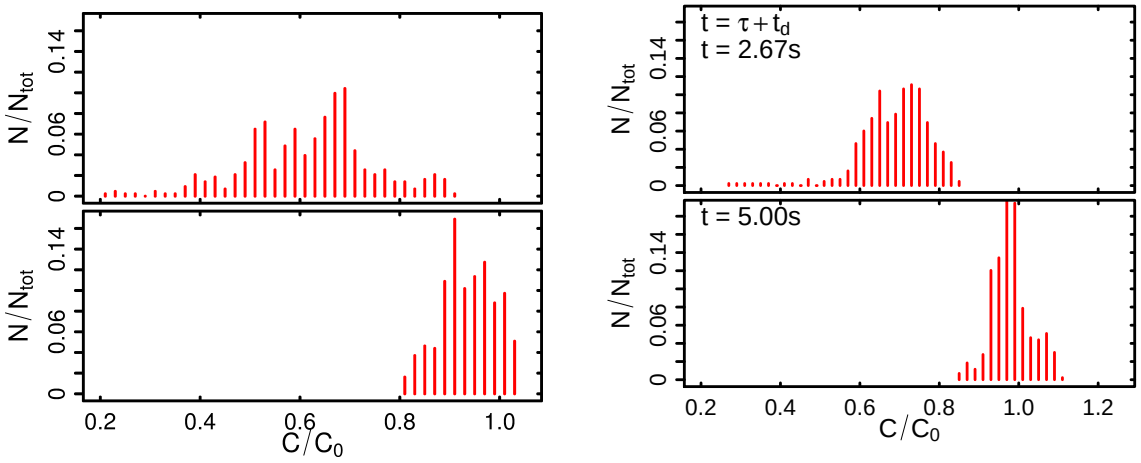

(a) (b)

Figure 19: Relative histogram of the concentration at outlet for $t = \tau(s)$ (top) and $t = 5s$, (a):WALE, (b):SST-SAS.

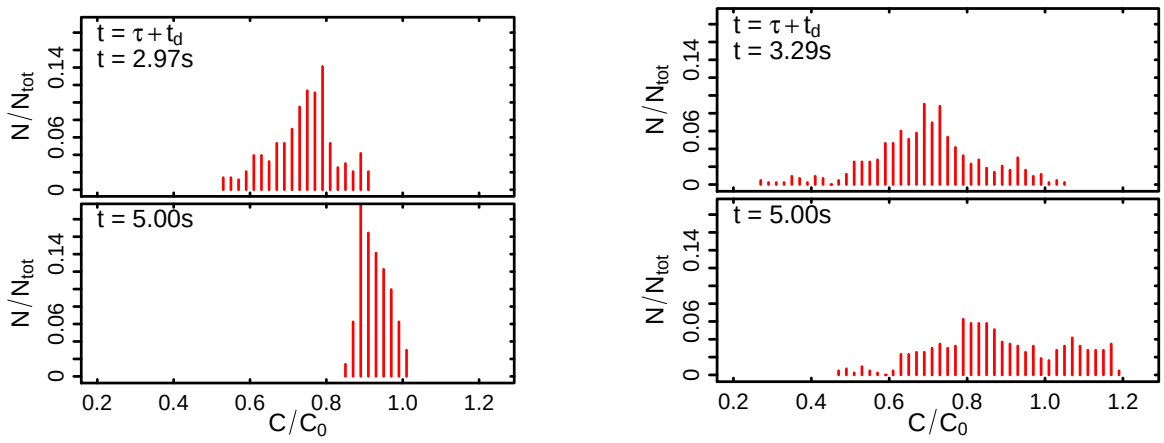

(a) (b)

Figure 20: Relative histogram of the concentration at outlet for $t = \tau(s)$ (top) and $t = 5s$, (a):SA-IDDES, (b):k-omega-DES.

7 Acknowledgment

The authors acknowledge the funding (partially) of this work by Deutsche Forschungs Gemeinschaft (DFG) under grant number SFB/TRR 129.

References

[1] F.R. Menter and Y. Egorov "The scale adaptive simulation method for unsteady turbulent flow prediction, Part 1: Theory and Model Description." *Flow Turbul. Combust* **85**, 113–138. DOI: 10.1007/s10494-010-9264-5, (2010).

[2] F.R. Menter, J. Sch¨utze, and M. Gritskevich "Global vs. Zonal Approaches in Hybrid RANS-LES Turbulence Modeling." *4th Symposium on Hybrid RANS-LES Methods, Beijing*, (2011)

[3] A. Mehdizadeh, H. Foroutan, G. Vijayakumar and A. Sadiki. "A new formulation of scale adaptive simulation approach to predict complex wall bounded shear flows" *Journal of Turbulence*, **15/10**, 629-649, (2014)

[4] A. Mehdizadeh, J.G. Brasseur, T. Nandi and H. Foroutan. "Analysis of Scale Adaptive Approaches Based on the Rotta Transport Equation" *Notes on Numerical Fluid Mechanics and Multidisciplinary Design 130*, DOI 10.1007/978-3-319-15141-0-23, (2015)

[5] Girimaji S., Haase W., Peng S. H. and Schwamborn, D., *"Notes on numerical fluid mechanics and multidisciplinary design 130"*, Springer International Publishing Switzerland, (2015)

[6] Mikhail L. Shur, Philippe R. Spalart, Mikhail Kh. Strelets, and Andrey K. Travin "A hybrid RANS-LES approach with delayed-DES and wall modelled LES capabilities" *International Journal of Heats and Fluid Flow, 29:1638–1649*, (2008)

[7] P. Spalart., "Detached-eddy simulation" *Annual Review Fluid Mechanics*, **41**, 181—202, (2009)

[8] P. Spalart and S. R. Allmaras "A one-equation turbulence model for aerodynamic flows." *La Recherche Aerospatiale, 1:5–21*, (1994)

[9] P. Spalart, WH Jou, M Strelets, and SR Allmaras "Comments on the feasibility of les for wings, and on a hybrid rans/les approach" *Advances in DNS/LES, 1:4–8*, (1997)

[10] P. Spalart, S. Deck,M.L. Shur, K.D. Squires, M. Kh. Strelets, and A.K. Travin "A new formulation of detached eddy simulation, resistant to ambiguous grid densities" *Theoritical and Computational Fluid Dynamics*, **20(3)**, 181–195, (2006)

[11] Rotta, J.C.:Turbulente Stroemungen. *Teuber Verlag*, (1972).

[12] F. Menter, "Two-equation eddy-viscosity turbulence model for engineering applications." *AIAA Journal*, **32**. 1598–1605 (1994)

[13] Available at *www.openfoam.com.*

[14] Toporov D., Bocian P., Heil P., Kellermann A., Stadler H., Tschunko S., Foerster M., Kneer R. "Detailed investigation of a pulverized fuel swirl flame in CO2/O2 atmosphere." *Combustion and Flame*, **vol 155**, 605-618 (2008).

[15] British Petroleum. BP Statistical Review of World Energy, *Nuclear Energy*, **www.bp.com/statisticalreview,** (2014). ISSN 02768739, doi: 10.2307/3324639.

[16] World Energy Outlook 2015 Factsheet, *Technical report*, (2015).

[17] S. Doost, F. Ries, L. Becker, S. Buerkle, S. Wagner, V. Ebert, A. Dreizler, F. Dimare, A. Sadiki and J. Janicka " Residence Time Calculations in Complex Swirled Turbulent Flow in Combustion Chambers Using Large-Eddy Simulations", *Chemical Engineering Science 156*, 97-114, (2016).

[18] F.R. Menter, *"Best Practice-Scale-Resolving Simulations in ANSYS CFD - Application Brief, Version 2.0"*, http://resource.ansys.com, (2015)

[19] K. Hanjalic, "Will RANS Survive LES? A View of Perspectives" *Journal of Fluid Engineering*, DOI:10.1115/1.2037084 (2005)

[20] B. Kniesner, S. Saric, A. Mehdizadeh., S. Jakirlic, K. Hanjalic, C. Tropea, D. Sternel, F. Gauss and M. Schaefer, "Wall Treatment in LES by RANS Models, Method Development and Application to Aerodynamic Flows and Swirl Combustors", *ERCOFTAC Bulletin, 72*, 33–40, (2007).

[21] F.R. Menter, M. Kuntz, and R. Langtry, "Ten years of industrial experience with the SST turbulence model" *In Proceedings of the fourth international symposium on turbulence, heat and mass transfer*, pp 625-–632, Antalya, Turkey, (2003).

[22] K. Hanjali´c, D. Borello, G. Delibra and F. Rispoli, "Hybrid LES/RANS of Internal Flows: A Case for More Advanced RANS" *Progress in Hybrid RANS-LES Modelling,Notes on Numerical Fluid Mechanics and Multidisciplinary Design 130*, DOI 10.1007/978-3-319-15141-0-2, (2015).

[23] O. Keck, W. Meier, W. Stricker, and M. Aigner, "Establishment of a confined swirling natural gas/air flame as a standard flame: temperature and species distributions from laser raman measurements" *Combust. Sci.and Tech.*, 174(3):117–151, (2002).

[24] T. Landenfeld, A. Kremer, E.P. Hassel, J. Janicka, T. Sch¨a, J. Kazenwadel, "C. Schulz, and J. Wolfrum. Laserdiagnostic and numerical studies of strongly swirling natural gas flames", *Proceedings of the Combustion Institute*, 27:1023–1030, (1998).

[25] G. Scheffknecht, L. Al-Makhadmeh, U. Schnell and J. Maier, " Oxy-fuel coal combustion—A review of the current state-of-the-art" *International Journal of Greenhouse Gas Control*, **5**, pp. 16–35, (2011)

[26] E. Palkin, R. Mullyadzhanov1, M. Hadziabdic and K. Hanjalic, "Scrutinizing URANS in Shedding Flows: The Case of Cylinder in Cross-Flow in the Subcritical Regime" *Flow Turbulence Combust*, DOI: 10.1007/s10494-016-9772-z, (2016)

[27] U. Piomelli, "Large eddy simulations in 2030 and beyond" *Phil. Trans. R. Soc. A*, 372(2022), 20130320, (2014)

[28] J. Hagen, "Chemiereaktoren, Auslegung und Simulation" *Wiley-VCH, Weinheim*, (2004)

[29] F. Nicoud and F. Ducros, "Subgrid-scale stress modelling based on the square of the velocity gradient tensor" *Flow Turbul. Combust*, 62(3), (1999)

[30] S. Bürkle, L.G. Becker, M. A. Agizza, A. Dreizler, V. Ebert, and S. Wagner, "In-situ measurement of residence time distributions in a turbulent oxy-fuel gas-flame combustor." *Experiments in Fluids*, 58(7), 77, (2017)

[31] K. Koeckler, S. Terhaar, and C. Oliver Paschereit, "Residence time distribution in a swirling flow at nonreacting, reacting, and steam-diluted conditions." *J. Eng. GasTurb. Power*, 136, 41505, (2014)

[32] O. Levenspiel, "Chemical reaction engineering." *3rd ed. Wiley New York*, (1999)

[33] M. Costa, P. Silva, and J.L.T. Azevendo, "Measurements of gas species, temperature, and char burnout in a low-nox pulverized-coal-fired utility boiler." *Combust. Sci. Technol.*, 175(2), 271–289, (2003)

[34] P.R. Van Der Lans, P. Glarborg, K. Dam-Johanson and P. S. Larsen, "Residence time distribution in a cold, confined swirl flow, Implications for chemical engineering combustion modelling." *Chem. Eng. Sci.*, 52(16), 2743–2756, (1997)

[35] J. Froelich, D. von Terzi "Hybrid LES/RANS Methods for the Simulation of Turbulent Flows." *Progress in Aerospace Science*, 44/5, 349–377, (2008)

[36] D.B. Spalding, "A single formula for the law of the wall." *J.Appl.Mech.*, 28/3, 455, (1961)

90

Appendix A

WALE Model

In classical LES techniques only large scale structures are resolved containing most of the turbulent kinetic energy while small scale motions need to be modeled.The resulting filtered conservation equations for mass and momentum are written in conservative form as below:

$$\frac{\partial \tilde{u_i}}{\partial x_i} = 0,$$

$$\frac{\partial \tilde{u_i}}{\partial t} + \tilde{u_j}\frac{\tilde{u_i}}{\partial x_j} = -\frac{\partial \tilde{P}}{\partial x_i} + \frac{\partial}{\partial x_j}\left(\nu\left(\frac{\partial \tilde{u_i}}{\partial x_j} + \frac{\partial \tilde{u_j}}{\partial x_i}\right)\right) - \frac{\partial \tau_{ij}^{sgs}}{\partial x_j},$$

where $\tilde{u_i}$, $\tilde{P}$,ν and τ_{ij}^{sgs} are filtered velocity, filtered pressure, kinematic viscosity and unknown sub-grid scale (SGS) stress tensor respectively. Following Boussinesq approximation, the sub-grid stress tensor is modeled as follows:

$$\tau_{ij}^{sgs} = \frac{2}{3}k\delta_{ij} - \nu_t\left(\frac{\partial \tilde{u_i}}{\partial x_j} + \frac{\partial \tilde{u_j}}{\partial x_i}\right),$$

where k is sub-grid scale turbulent kinetic energy and nu_t is the SGS eddy viscosity. Following WALE model[29], the turbulent SGS eddy viscosity ν_t is expressed as below:

$$\nu_t = (C_w\Delta)^2\frac{\left(\mathbf{S}_{ij}^d\mathbf{S}_{ij}^d\right)^{3/2}}{\left(\bar{S}_{ij}\bar{S}_{ij}\right)^{5/2} + \left(\mathbf{S}_{ij}^d\mathbf{S}_{ij}^d\right)^{5/4}},$$

where C_w is a true dimensionless constant (in the present study $C_w = 0.325$), $\Delta = (\Delta_x\Delta_y\Delta_z)^{1/3}$ the characteristic cutoff length scale of the grid filter, $\bar{S}_{ij}$ the filtered strain rate tensor defined as $\bar{S}_{ij} = \frac{1}{2}\left(\frac{\partial \bar{u}_i}{\partial x_j} + \frac{\partial \bar{u}_j}{\partial x_i}\right)$ and $\mathbf{S}_{ij}^d$ the traceless symmetric part of the square of the velocity gradient tensor defined as

$$\mathbf{S}_{ij}^d = \frac{1}{2}\left(g_{ij}^2 + g_{ji}^2\right) - \frac{1}{3}\delta_{ij}g_{kk}^2,$$

where $g_{ij}^2 = g_{ik}g_{kj}$ is the square of the filtered velocity gradient tensor $g_{ij} = \partial\bar{u}_i/\partial x_j$. One of the advantages of this model is the production of zero turbulent eddy-viscosity in the vicinity of a wall.

In the present study the wall-shear stress model based on the universal law of the wall suggested by [36] is applied for near-wall treatment. Thereby, the velocity profiles are well fitted for the laminar, buffer and logarithmic regions of an equilibrium boundary layer by the formula

$$y^+ = u^+ + \frac{1}{E}\left(e^{\kappa u^+} - 1 - \kappa u^+ - \frac{1}{2}(\kappa u^+)^2 - \frac{1}{6}(\kappa u^+)^3\right),$$

where y^+ denotes the wall coordinate, which is the distance to the wall y_p made dimensionless with the shear velocity u_τ and the kinematic viscosity ν ($y^+ = \frac{y_p u_\tau}{\nu}$), u^+ represents the dimensionless velocity, which is the velocity u_p parallel to the wall divided by the shear velocity u_τ ($u^+ = \frac{u_p}{u_\tau}$), κ is the Kármán constant ($\kappa = 0.41$) and E an empiric constant ($E = 9.1$).

To provide the wall shear velocity u_τ Eq. (10) can be transformed into a non-linear equation for u_τ by substituting the known values y_p and u_p.

These kinds of stress equilibrium wall functions have the inherent limitation being valid only in zero pressure gradient equilibrium flows. This limitation is met in the investigated setup configuration as there is no demand to account for any effects of pressure gradient on the near-wall velocity profile.

Appendix B

The $k-\omega-SST-SAS$ Model

The governing equations for $k-\omega-SST-SAS$ model reads as follows[1]:

$$\frac{\partial k}{partialt} + \frac{\partial U_i k}{\partial x_i} = P_k - \beta^* \omega k + \frac{\partial}{partial x_i}\left((\nu + \sigma_k \nu_t)\frac{\partial k}{\partial x_i}\right),$$

$$\frac{\partial \omega}{\partial t} + \frac{\partial U_i \omega}{\partial x_i} = \alpha S^2 - \beta \omega^2 + \frac{\partial}{\partial x_i}\left((\nu + \sigma_\omega \nu_t)\frac{\partial \omega}{\partial x_i}\right) + 2(1-F_1)\sigma_{\omega 2}\frac{1}{\omega}\frac{\partial k}{\partial x_i}\frac{\partial \omega}{\partial x_i} + Q_{SAS}.$$

$$\nu_t = \frac{a_1 k}{max(a_1\omega, SF_2)},$$

where $P_k = min(\nu_t S^2, 10\beta^* k\omega)$ and S production of turbulent kinetic energy and invariant of the strain rate tensor respectively. Q_{SAS} is the triggering mechanism and is defined and discussed in detail in section 2.1.

The blending functions F_1 and F_2 are defined as follows:

$$F_1 = tanh\left\{\left\{min\left[max(\frac{\sqrt{k}}{\beta^*\omega y}, \frac{500\nu}{y^2\omega}), \frac{4\rho\sigma_{\omega 2}k}{CDy^2}\right]\right\}^4\right\},$$

$$F_2 = tanh\left[\left[max\left(\frac{2\sqrt{k}}{\beta^*\omega y}, \frac{500\nu}{\omega y^2}\right)\right]^2\right],$$

where y is the distance from the nearest solid wall.

CD is defined as below:

$$CD = max\left(2\rho\sigma_{\omega 2}\frac{1}{\omega}\frac{\partial k}{\partial x_i}\frac{\partial \omega}{\partial x_i}, 10^{-10}\right).$$

All model constants are computed by a blend as follows:

$\phi = F_1\phi_1 + (1 - F_1)\phi_2$ with the model constants in the following:

$\sigma_{k1} = 0.85$, $\sigma_{k2} = 1$, $\sigma_{\omega 1} = 0.5$, $\sigma_{\omega 2} = 0.856$, $\beta_1 = 0.075$, $\beta_2 = 0.0828$, $\beta^* = 0.09$, $\alpha_1 = 0.555$, $\alpha_2 = 0.44$, $a_1 = 0.31$.